ACS EARTH AND SPACE CHEMISTRY

http://pubs.acs.org/journal/aesccq

Article

Sources, Composition, and Mixing State of Submicron Particulates over the Central Indo-Gangetic Plain

Nandita Singh, Tirthankar Banerjee,* Karine Deboudt, Abhishek Chakraborty, Md Firoz Khan, and Mohd Talib Latif

Cite This: *ACS Earth Space Chem.* 2021, 5, 2052−2065

Read Online

ACCESS | Metrics & More | Article Recommendations | Supporting Information

ABSTRACT: Submicron particulates, collected between 2015 and 2018 in an urban environment over the central Indo-Gangetic Plain, South Asia, were analyzed. Particulate concentration was typically high during winter (DJF, 115 ± 50 $\mu g\ m^{-3}$) and post-monsoon seasons (ON, 79 ± 52 $\mu g\ m^{-3}$). Submicron particulates constituted a major fraction (69%) of fine particulates ($PM_{2.1}$) without much seasonal discrepancies. Particulates were metal-enriched (17 ± 6%) with signature of crustal and road dust resuspensions. Metal enrichment was evident specifically for Zn, Co, and Cr. Sulfate was the most robust ion contributing 10% (±4%) of particulate mass followed by nitrate (6 ± 3%) and ammonium (4 ± 2%). Overall, water-soluble ions accounted for one-third of particulate mass mainly comprised secondary ones. The *n*-alkane homologues (C_{17}−C_{35}) showed prevalence of low-molecular-weight (LMW) alkanes ($<C_{25}$) with the carbon preference index (CPI) close to one (1.3 ± 0.3) referring predominant contribution of burning of fossil fuels. Similarly, prevalence of LMW fatty acids ($\leq C_{20}$) with a high CPI (9.9) indicates emissions from residential cooking. The presence of dicarboxylic acids and phthalates with a vital signature of anthropogenic emissions was also traced. Strong enrichment of levoglucosan (600 ± 388 ng m^{-3}) was noted especially during peak biomass-burning episodes. Single-particle analysis indicates high abundance of carbonaceous particles (CPs) having both chain-like soot spherules and amorphous tar balls. These CPs were mostly pure, externally mixed against secondary particles for which the mixing state varied among the seasons. Source apportionment by an advanced receptor model indicates secondary aerosols and biomass-burning emissions as the major sources of submicron aerosols (43%), followed by resuspensions of mineral dusts (18%) and emissions from refuse/waste combustion (18%).

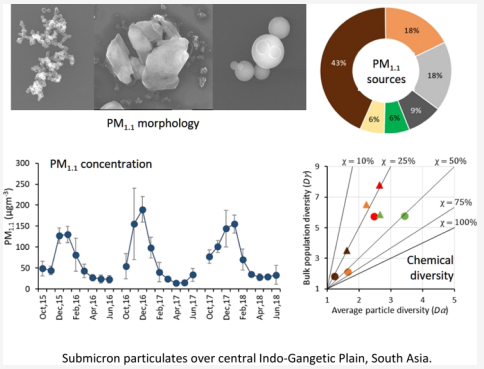

KEYWORDS: *inorganic species, levoglucosan, mixing state, receptor model, secondary aerosols*

1. INTRODUCTION

Exposure to air pollution has been recognized as a major global environmental threat to human health and has been linked to many premature mortality and health complications.[1,2] In most of the cases, air pollution-based epidemiological studies consider exposure to airborne particulate to quantify health risks which typically varies for different particulate sizes and associated sources.[3] Besides health risks, possible association between airborne particulates and biogeochemistry of nutrients,[4] climate change/variability,[5,6] cloud modifications,[7] thereby its impact on hydrological cycle[8] especially on Indian monsoon,[9] and on food security has also been explored.[10,11] Quantifying particulates' climate feedback pose considerable uncertainties especially due to the variations in particulate sources, composition, morphology, and mixing states. While the evidence of differential implications is far from conclusive, it is often projected that the size of the particulates and the kinds of sources such as combustion, crustal, marine, and biogenic govern the fundamental properties of particulates and their implications on the receptor site.

Among many particulate size groups, research on atmospheric chemistry and sources of submicron particulates (PM_1, with aerodynamic diameter ≤ 1.0 μm) is limited and inconsistent. There are growing interests on identifying number, mass concentration, and chemistry of submicron particulates with possible health effects. Submicron particulates constitute the major fraction of total particulate mass and number concentration[12] and essentially regulate atmospheric chemistry and climate-governing properties of aerosols. These particulates are typically carbonaceous in nature with fractions of metallic species and secondary ions; however, constituents and evolution vary based on its sources, meteorology, and aging process.[13,14] Submicron particulates are a typical product

Received: May 6, 2021
Revised: June 28, 2021
Accepted: July 28, 2021
Published: August 10, 2021

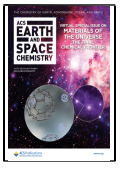

https://doi.org/10.1021/acsearthspacechem.1c00130
ACS Earth Space Chem. 2021, 5, 2052−2065

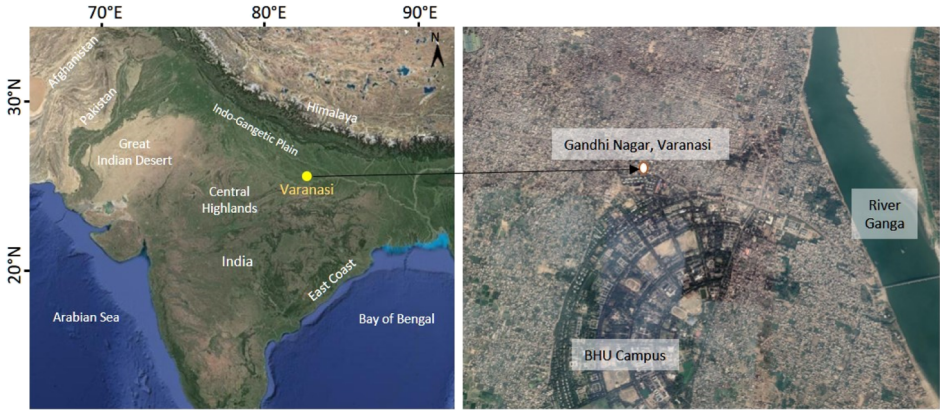

Figure 1. Geographical location of the particulate monitoring station.

of combustion processes which include residential and commercial biomass/waste-burning, transport, and industrial emissions and from burning of agriculture residues. However, gas-to-particle conversion, construction activities, and resuspensions of mineral dusts also generate submicron particulates.[13,15,16] There are explicit pieces of evidence that PM_1 efficiently travels through the human lungs, inducing inflammatory responses, causing oxidative damages to living cells, particularly acinar lung, and activating the immune system.[17] Besides, exposure to PM_1 is also linked to many other health complications particularly for cardiovascular, cerebrovascular, and ischemic heart disease with enhanced mortality and morbidity.[18,19]

Studies on submicron particulate chemistry and sources are sparse over South Asia, constrained especially by the limitation and uncertainty in PM_1 measurement. Within South Asia, the Indo-Gangetic Plain (IGP) shares the maximum burden of particulate pollution;[20,21] particulates which are reported to be highly mixed,[22−24] composed primarily of organics and secondary inorganics[13,25−27] with diverse kinds of sources.[28,29] Until the submission of the manuscript, very few studies explored submicron particulate chemistry over the IGP, focusing mainly over the urban agglomerates with emphasis on particulate composition and sources,[30] influence of fog processing,[13] and formation of secondary organics.[25,31] These studies essentially focus on season- or event-specific aerosol chemistry with none explicitly considering particulate exposure data for a longer period. Besides, very few studies explored submicron particulate morphology and mixing state leaving considerable uncertainties about their possible climate and health implications. The mixing state of submicron particulates can strongly regulate aerosol−radiation interaction and aerosol potency to serve as cloud condensation nuclei.[32] Considering the evidence of highly diverse airborne particulates across the IGP with many aerosol precursors and trace gases, it seems necessary to address these issues for better climate prediction and air quality modeling.

Here, we have examined a 3 year-long submicron particulate monitoring database from an urban background over the central IGP and characterized particulate-bound elements, water-soluble ions, and organics constrained by different seasons. We have explored mechanisms to establish the contamination factor (CF) and pollution index of heavy metals, provide insights on ionic balance and neutralization of submicron aerosol acidity, and include pieces of evidences on the secondary nature of aerosol organics. Individual particle morphology and mixing states have been reported for the first time over the region with an explanation on their possible formation pathway and climatic implications. Besides, we have used an advanced receptor model to apportion the sources of submicron particulates. Our analysis is novel for considering a large PM_1 monitoring database with information on multiple dimensions of particulate chemistry and mixing state which may well be useful to relate their possible implications on human health, regional climate, and ambient air quality.

2. METHODOLOGY

2.1. Monitoring Submicron Particulate. Monitoring of submicron particulates was performed in a residential area of Gandhi Nagar, Varanasi (25.28° N, 82.99° E, 81 m above sea level), located nearby the Banaras Hindu University campus (Figure 1). Detailed description of the sampling site and particulate monitoring procedure is mentioned in Singh *et al.*[27] In brief, ambient size-segregated particulates were collected for 72 h on prebaked quartz fiber filters at a height of 6 m using an eight-stage cascade impactor (Tisch Environmental TE-20-800) maintaining a flow rate of 28.3 L min^{-1}. Sampling was performed once a week continuously for 3 years (October 2015 to June 2018) except in monsoon months (July, August, and September). Among eight individual stages of the cascade impactor (with 50% collection efficiency), the last three stages having cutoff diameter ≤1.1 μm were combined and analyzed for submicron particulate ($PM_{1.1}$). From each daily aerosol sample, one-fourth was used for measuring ions and water-soluble organic carbon (WSOC), one-fourth for elements, and rest was used for organic extraction. For determining the microscopic properties of particulates, representative samples of size-segregated particulates were also collected for 3 to 5 h on copper transmission electron microscopy (TEM) grids (Ted Pella Inc.) and Nuclepore track-etch membranes (Whatman) depending on the particulate loading.

2.2. Bulk Chemical Analyses. *2.2.1. Solvent-Soluble Organic Compounds.* For analyzing the solvent-soluble organic compounds, the exposed filter composites were extracted by ultrasonication with solvent mixtures (v/v) hexane−dichloromethane (1:1), followed by methanol−dichloromethane (1:1). Both solvent extracts were pooled together and filtered through a 0.2 μm syringe filter. The filtered extract was concentrated via a vacuum rotatory evaporator up to 1 mL and finally reduced to 100 μL with a nitrogen concentrator.[33] The reduced extract was derivatized with *N,O*-bis-(trimethylsilyl)-trifluoroacetamide containing 1%

https://doi.org/10.1021/acsearthspacechem.1c00130
ACS Earth Space Chem. 2021, 5, 2052−2065

trimethylchlorosilane, and the final residue was redissolved in 1 mL of gas chromatography (GC)-grade hexane and analyzed with GC−mass spectrometry (GC−MS, QP2010 Ultra, Shimadzu, Japan). The GC−MS specifications and temperature program are mentioned in detail in Singh *et al.*[27] Briefly, samples were injected in GC−MS at 260 °C injector's temperature and column oven temperature program was begun at 50 °C (2 min isothermal hold), elevated linearly up to 120 °C for 4 min and next up to 300 °C for 30 min followed by an isothermal hold of 11 min at 300 °C. Molecular ions were produced using a 70 eV electron impact ionization technique and were extensively scanned for m/z ranging from 40 to 650. Compounds were identified on the basis of the mass fragmentation pattern from NIST library and from the reference standards. The blank filters were also treated similarly to the exposed filter samples for quality assurance.

2.2.2. Trace Elements. Analysis of particulate-bound element species was performed by following US EPA Method IO-3.2.[34] The exposed filters were cut into small pieces and digested with an extracting reagent (mixture of 5.55% HNO_3 and 16.67% HCl) for 2 h. Milli-Q water (resistivity: 18.2 MΩ cm) was added to the extraction residue, and the solution was filtered with Whatman no. 42 filters. The final filtrate was used for analyzing major metallic species (Na, K, Ca, Mg, Fe, and Zn) by inductively coupled plasma (ICP) optical emission spectrometry (iCAP 6300 DUO, Thermo Scientific) and trace elements (Cr, Mn, Cu, Pb, Ni, Co, and Cd) by ICP-mass spectrometry (300× NexION, PerkinElmer). The background contamination was reduced by performing blank correction and three-point calibration was used for quantification, prepared by certified reference standards. Standard recovery tests were performed and recovery efficiencies of all the metals varied in between 93% (Cu) and 100% (Ni).

2.2.3. Water-Soluble Inorganic Species. Particulate laden filters were processed for 90 min with Milli-Q water in an ultrasonicator for extracting water-soluble ions (Microclean-109, Oscar, India). The extracted solution was filtered through a 0.2 μm syringe filter and half portion of the filtrate was used for analyzing water-soluble inorganic species (WSIS). Rest half of the filter extract was stored and utilized for estimating WSOC. Water-soluble ions were analyzed using an ion-exchange chromatograph (ICS 3000, Dionex, USA). Anionic species (Cl^-, SO_4^{2-}, and NO_3^-) were separated using 20 mM NaOH (50% w/w) as an eluent on the analytical column (IonPac AS11-HC×250 mm) with a guard column (IonPac AG11-HC, 4 × 50 mm) and suppressor (AERS-300, 4 mm). Cations (NH_4^+, Na^+, K^+, Ca^{2+}, and Mg^{2+}) were separated using 5 mM methane sulfonic acid as an eluent on the analytical column (IonPac CS12A-HC, 4 × 250 mm) with a guard column (IonPac CG11-HC, 4 × 50 mm) and suppressor (CERS-300, 4 mm). Filter blank values for each ion were subtracted from sample values to remove any background contamination.

2.2.4. Water-Soluble Organic Carbon. WSOC was analyzed using the aqueous extract prepared for WSIS analysis. The total carbon and inorganic carbon contents of samples and filter blanks were analyzed using a total organic carbon analyzer (TOC-1200, Thermo ECN Corp.) following Kirillova *et al.*[35] Total WSOC was estimated by computing the difference between total carbon and inorganic carbon contents after blank correction.

2.3. Single-Particle Analyses and Aerosol Mixing State. Morphology and composition of individual particles were analyzed using a scanning electron microscope (JEOL 7100F) coupled with three energy-dispersive X-ray (EDX) detectors (Bruker X-Flash 6/30). The EDX spectra of particles were obtained at 15 kV accelerating voltage with a probe current of 200 pA and an acquisition period of 30 s. Automated analysis of particles was performed using Link Esprit software (Bruker), and atomic concentrations were achieved by PhiRhoZ quantification. Classification of different particle types was based on the percent weight ratio of the elements with $Z \geq 11$. A particle was classified as X-rich when the $P(\mathrm{X}) \geq 65\%$, and $P(\mathrm{X})$ of an element (X) was computed using the following equation[36]

$$P(\mathrm{X}) = \frac{\mathrm{X}}{\sum \mathrm{Na, Mg, Ca, Al, Si, S, Cl, K, Fe, Ti}} \times 100 \quad (1)$$

To understand the mixing state of submicron particles, species diversity parameters were initially calculated based on the mixing entropy concept introduced by Riemer and West.[37,38] These parameters were only assessed for winter (DJF) and pre-monsoon (MAMJ), hypothesizing distinct types of dominant sources and particle mixing state during these two periods, that is, biomass/waste/refuse burning in winter and crustal resuspensions in pre-monsoon season.[15,27] The concept and methodology for estimating the particle mixing state may be found in the works of Riemer and West,[37,38] while a brief description is included here. Initially, single-particle diversity which corresponds with the effective number of chemical elements within a particle was computed, before being applied to the entire particle population. The chemical diversity of entire particle population was then calculated in terms of α diversity ($D\alpha$), while the bulk population diversity was calculated in terms of γ diversity ($D\gamma$). The $D\alpha$ represents the average number of chemical elements per particle and $D\gamma$ indicates the effective number of elements in the bulk. These two diversities ($D\alpha$ and $D\gamma$) were used to estimate the mixing state index (χ) for different particle classes which provides insights on the homogeneity and heterogeneity of submicron aerosols. The mixing state index (χ) is a fractional value ranging from *zero*, when all particles are pure, *viz.,* composed of single species, that is, totally externally mixed population, to *one*, when all particles possess similar species mass fraction, that is, totally internally mixed population. The $D\alpha$ and $D\gamma$ diversities were computed using element mass fractions per particle obtained from EDX and the lower atomic number elements (C, N, and O) were not considered because of their interference from the substrate or detector.[37]

2.4. Source Apportionment of Particulates. For estimating the contribution of emission sources to submicron particulates, the positive matrix factorization (PMF 5.0, US EPA) model was used. PMF is a multivariate factor analysis based on the weighted least square approach that decomposes sample data measured at the receptor site into two matrices, *viz.,* factor profile (f) and factor contributions (g).[39] Each factor profile represents emission sources to the individual factor contribution in each sample and can be expressed as

$$x_{ij} = \sum_{k=1}^{p} g_{ik} f_{kj} + e_{ij} \quad (2)$$

where i denotes the sample in consideration, j is its chemical species, p is the number of factors contributing to the sample, x_{ij} denotes the concentrations associated to i by j matrix, and e_{ij}

https://doi.org/10.1021/acsearthspacechem.1c00130
ACS Earth Space Chem. 2021, 5, 2052−2065

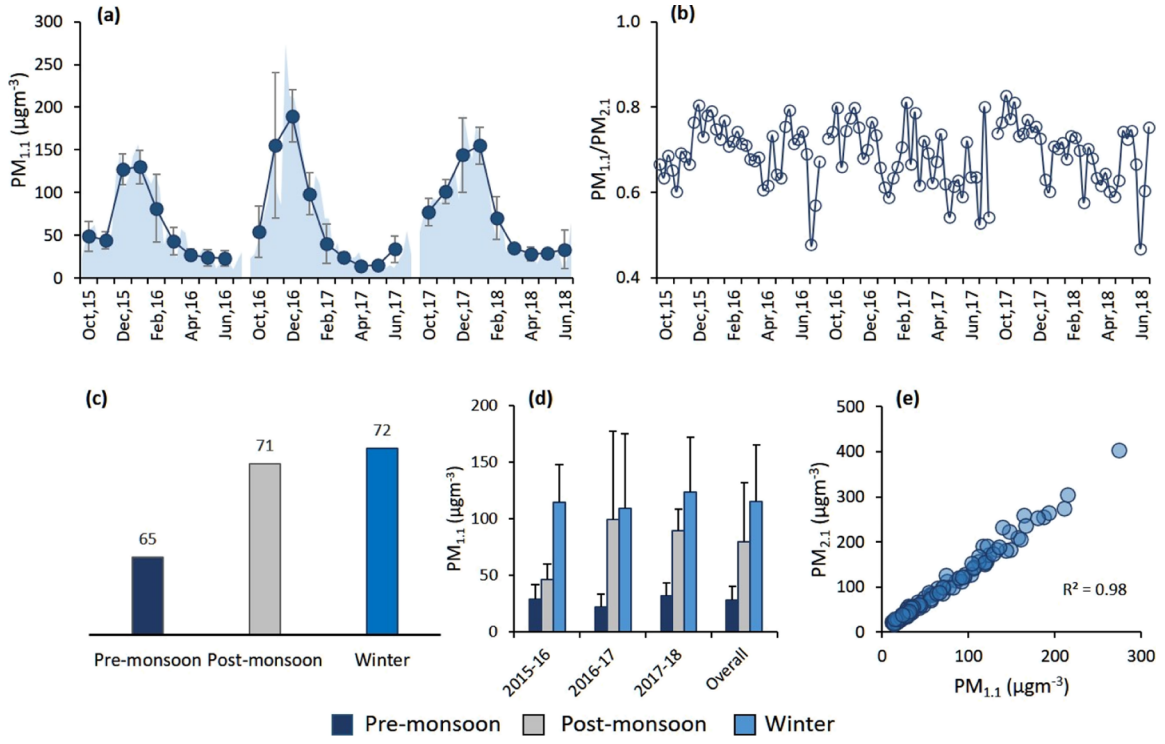

Figure 2. Variation in (a) mass concentration of submicron particulate, (b) $PM_{1.1}$ on $PM_{2.1}$ concentration ratio, (c) percent contribution of $PM_{1.1}$ to $PM_{2.1}$, (d) seasonal variations of $PM_{1.1}$ mass in each monitoring year, and (e) $PM_{1.1}$ as a function of $PM_{2.1}$.

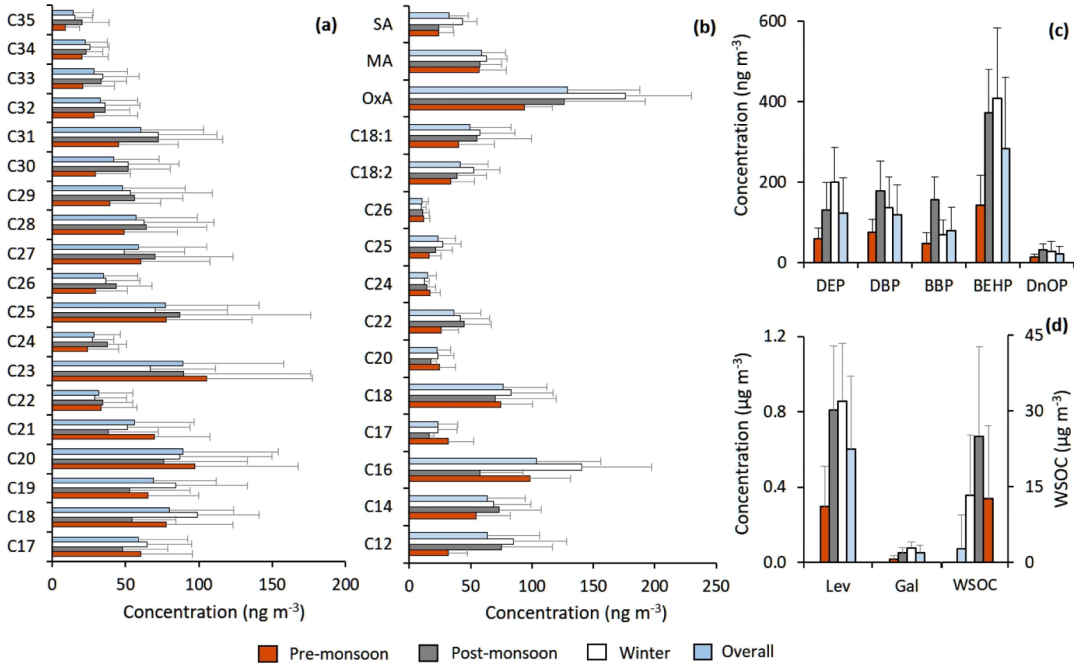

Figure 3. Molecular distribution of (a) *n*-alkanes, (b) fatty acids and dicarboxylic acids (DCAs), (c) phthalates, and (d) anhydrosugars and WSOC in submicron particulates.

represents the species residuals. The model input includes the measured particulate composition and associated uncertainty data at the receptor site. Uncertainty (U) associated with each chemical species measured above the method detection limit (MDL) was computed using the following equation

$$U = \sqrt{(\text{error fraction} \times \text{concentration})^2 + (0.5 \times \text{MDL})^2} \quad (3)$$

Species concentration measured below the MDL was replaced by half of its MDL value and associated uncertainty was replaced by 5/6 times of MDL.[27,39] Missing observations were replaced by the median value of the respective species, and associated uncertainty was substituted by four times of the species median value.[27] The model was simulated using 112 samples including 58 chemical species with 5% additional modeling uncertainty. In order to achieve the most

https://doi.org/10.1021/acsearthspacechem.1c00130
ACS Earth Space Chem. 2021, 5, 2052−2065

representative source apportionment result, PMF was first optimized with 3 to 7 factors and the optimum number of factors was selected on the basis of goodness of fit.

3. RESULTS AND DISCUSSION

3.1. Particulate Mass Concentration. Figure 2a provides the variations in 72 h mean $PM_{1.1}$ mass concentration monitored in between October 2015 to June 2018 (*N*: 112) with descriptive statistics included in Table S1. Annual mean $PM_{1.1}$ concentration reached 69 (±55) $\mu g\ m^{-3}$ (median: 47; inter quartile range, IQR: 28−106 $\mu g\ m^{-3}$), with a season-specific high concentration during winter (DJF, *N*: 38; 115 ± 50 $\mu g\ m^{-3}$) followed by post-monsoon (ON, *N*: 25; 79 ± 52 $\mu g\ m^{-3}$). In contrast, mean concentration during pre-monsoon was relatively low (MAMJ, *N*: 49; 28 ± 12 $\mu g\ m^{-3}$). A season-specific high concentration during typical winter and post-monsoon months relates its possible emissions from the combustion sources, associated to burning of biomass, waste/refuse incineration, and from residential/commercial emission sources.[13,40] We also note that for 39% of monitoring events, measured $PM_{1.1}$ concentrations were higher than the annual mean of $PM_{1.1}$ (69 $\mu g\ m^{-3}$); all occurring in between October and February months, whereas for 92% of cases, concentration reached ≥100 $\mu g\ m^{-3}$, exclusively during early winter months (December−January). Measured $PM_{1.1}$ was reasonably low against the concentration in Kanpur (133−160 $\mu g\ m^{-3}$),[30] an industrial city in the central IGP; Delhi, the national capital (87 $\mu g\ m^{-3}$);[41] and many of the Chinese cities, where exceptionally high PM_1 concentration is reported.[42,43] However, measured $PM_{1.1}$ concentration in Varanasi was significantly high compared to other global cities, for example, Krakow, Poland (7−17 $\mu g\ m^{-3}$),[44] and Edmonton, Canada (17 $\mu g\ m^{-3}$).[16]

Variation in $PM_{1.1}$ against fine particulate mass ($PM_{2.1}$, as in Singh *et al.*[27]) is also included in Figure 2b,c. The $PM_{1.1}$-to-$PM_{2.1}$ ratio time series slightly declined during pre-monsoon (0.65 ± 0.01) compared to annual mean (0.69 ± 0.02), with the ratio remaining consistently high during winter (0.71 ± 0.06) and in post-monsoon months (0.72 ± 0.06). Overall, submicron particulates contribute 69% of fine particulate mass with very high R^2 (0.98; Figure 2e) between $PM_{1.1}$ and $PM_{2.1}$, depicting resemblance of the sources. The findings were in accordance to the reported observation over China where the major fraction of fine particulates consisted of submicron aerosols and PM_1-to-$PM_{2.5}$ ratio increases exclusively during high pollution days.[42]

3.2. Composition of Particulate Organics. Figure 3 includes variations in particulate-bound homologous series of *n*-alkanes (C_{17}−C_{35}), fatty acids (C_{12}−C_{26}), dicarboxylic acids, phthalates, and anhydrosugars and their molecular distributions. Summary of the concentrations of individual molecules is included in Table S1, and seasonal differences in various organic groups along with diagnostic ratios are given in Table S2. The list of abbreviations used for different organic molecules is included in Table S3. It should be noted that molecular characterization of $PM_{1.1}$-bound organic aerosols (in terms of alkanes, carboxylic and fatty acids, and phthalates) are being reported for the first time over the IGP, therefore, remain mostly incomparable.

3.2.1. n-Alkanes. Overall mean (±SD) concentration of 19 homologous solvent-extracted *n*-alkanes was 0.98 (±0.50) $\mu g\ m^{-3}$. Concentration varied insignificantly among the seasons with slight abundance during post-monsoon and winter compared to summer months. Molecular distribution of *n*-alkanes indicates that in most of the cases, C_{max} was at C_{23}. Besides, concentration of low-molecular-weight (LMW, $<C_{25}$) *n*-alkanes was 1.7 (±0.8) times higher than that of high-molecular-weight (HMW) *n*-alkanes, indicating dominance of fossil fuel-burning emissions against biogenic emissions (including both epicuticular wax and biomass burning). A weak dominance of odd-numbered *n*-alkanes was also found both in LMW and HMW alkanes. The carbon preference index (CPI) remained close to unity (1.3 ± 0.3) with insignificant seasonal variations (1.2−1.4), reaffirming the major source of contributions from partial combustion of petroleum residues and fossil fuels.[45,46] We also note that LMW *n*-alkanes were having high CPI (1.5 ± 0.4) against the HMW compounds (1.1 ± 0.3).

3.2.2. Fatty Acids. Fatty acids (C_{12}−C_{26}) including unsaturated oleic ($C_{18:1}$) and linoleic acid ($C_{18:2}$) were also traced in submicron aerosols over the central IGP. Fatty acids were particularly abundant during winter with a mean concentration of 0.62 (±0.13) $\mu g\ m^{-3}$ against an overall mean of 0.49 (±0.17) $\mu g\ m^{-3}$. Molecular distribution of fatty acids indicates prevalence of LMW acids ($\leq C_{20}$) with very high LMW-to-HMW fatty acid ratio (9.3 ± 7.0). In general, LMW fatty acids are mainly anthropogenic (sources including vehicular exhausts, residential cooking, and burning of biomass), while HMW fatty acids are predominately biogenic (sources such as waxy leaf surface abrasions and wood smoke).[46,47] The LMW/HMW ratio remained particularly high during pre-monsoon months (11.8 ± 8.4) mainly due to the reduced contribution of biogenic sources including wood smoke emissions. The mean CPI of fatty acids was 9.9 (±5.4), slightly high during pre-monsoon (11.5 ± 6.5) against rest of the seasons (8.4−9.7). Molecular distribution clearly demonstrates prevalence of even carbon fatty acids in $PM_{1.1}$ with C_{max} at $C_{16:0}$ (*n*-hexadecanoic acids), followed by $C_{18:0}$ (*n*-octadecanoic acids). The ratio of $C_{18:0}$ to $C_{16:0}$ remained 0.9 (±0.5), exclusively high during winter (1.3 ± 0.6) refereeing emissions predominately from residential cooking and resuspensions from paved and unpaved road dust.[27,48] We also found evidence that part of submicron particulates are more aged (typically transported aerosols) as the ratio between C_{sat} [$C_{(18:0+16:0)}$] and C_{unsat} [$C_{(18:n+16:1)}$] fatty acids was high (2.8 ± 3.0) compared to the reported ratio for fine (1.3) and coarser particulates (1.7) for the same monitoring station.[27] However, this was more evident during the pre-monsoon period (3.7 ± 4.1) in contrast to post-monsoon and winter when relatively fresh aerosols of local origin dominate.

3.2.3. Dicarboxylic Acids. Three $PM_{1.1}$-bound DCA, namely, oxalic acid (C_2), malonic acid (C_3), and succinic acid (C_4) were detected. These are the typical secondary organic compounds emitted from vehicular/industrial emissions, biomass/waste-burning emissions and from photo-oxidation of volatile organic compounds (VOCs). Mean (±SD) DCA concentration was 213 (±82) $ng\ m^{-3}$ with characteristic wintertime high and summertime low abundance, primarily contributed by the oxalic and malonic acids. Overall, oxalic acids contributed 58% of total detected DCA and 27% by malonic acids with typical high concentrations during extreme biomass-burning events.

3.2.4. Phthalates. Here, five types of $PM_{1.1}$-bound phthalates, namely, diethyl phthalate (DEP), di-butyl phthalate (DBP), butyl benzyl phthalate, bis(2-ethylhexylphthalate) (BEHP), and di-*n*-octyl phthalate, were traced. Among these,

https://doi.org/10.1021/acsearthspacechem.1c00130
ACS Earth Space Chem. 2021, 5, 2052−2065

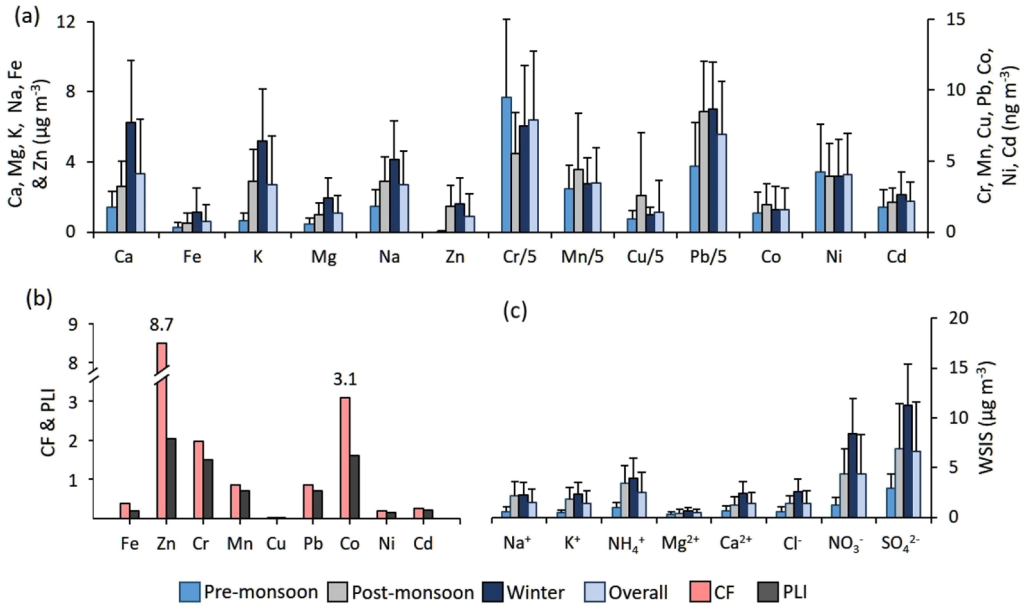

Figure 4. Variations in (a) element concentration, (b) CF and pollution load index (PLI), and (c) WSIS concentration in submicron particulates. Note: To maintain a similar scale in between trace elements, concentrations of Cr, Mn, Cu, and Pb are shown in 1/5 times.

BEHP is typically abundant in $PM_{1.1}$, while traces of DBP and BEHP are also reported in aerosols with sources including burning of different plasticizers/waste plastics and tail-pipe emissions from automobiles and from industrial sources.[49] Phthalate concentrations were normally high during winter (839 ± 326 ng m^{-3}) and post-monsoon seasons (871 ± 240 ng m^{-3}) against an annual mean of 625 (±346) ng m^{-3}. The presence of phthalates was also identified in fine particulates ($PM_{2.5}$), both in Varanasi (965 ± 504 ng m^{-3})[27] and New Delhi (130−210 ng m^{-3}).[49] Among the types, BEHP (283 ± 177 ng m^{-3}) was highly enriched in $PM_{1.1}$, followed by DEP (123 ± 88 ng m^{-3}), predominantly in winter, with possible sources including poly-vinyl chloride, coatings and varnishes, and emissions from their combustion.

3.2.5. Anhydrosugars. The presence of anhydrosugars was also detected in submicron particulates having very high abundance during winter (935 ± 323 ng m^{-3}) and post-monsoon seasons (857 ± 368 ng m^{-3}) with an annual mean concentration of 641 (±421) ng m^{-3}. Levoglucosan, a universal biomarker of biomass-burning aerosols, chiefly emits from the combustion of plant-based material such as cellulose and hemicellulose.[45,50] Levoglucosan constitutes the major fraction (92−95%) of traceable anhydrosugars, with an annual mean concentration of 600 (±388) ng m^{-3} (IQR: 251−932 ng m^{-3}). Measured $PM_{1.1}$-bound levoglucosan is well-comparable to the previous $PM_{2.5}$-based observations across the IGP, for example, in Kanpur (1363−1853 ng m^{-3}),[51] New Delhi (1978 ng m^{-3}),[52] Varanasi ($PM_{1.1}$: 649 ng m^{-3}),[45] and in other Asian cities, for example, Mt. Tai, China (391 ng m^{-3}),[53] and Beijing, China (590 ng m^{-3}).[50] Among the other isomers, galactosan was traced in $PM_{1.1}$, but mannosan remained undetected. The mean ratio of levoglucosan to galactosan was 21.9 (±16.7), with IQR varying from 9.8 to 30.1 and all the high values (≥10) typically noted during the peak biomass-burning period (October−February). Such a high ratio essentially indicates emissions of submicron aerosols from the burning of crop residues and hardwood which are conventionally used for residential cooking and heating purposes.[40]

3.2.6. WSOC. WSOC contributed 15% (±7) of $PM_{1.1}$ mass, slightly high during winter (21 ± 6%) compared to summer months (10 ± 5%). Relative concentration of WSOC varied in between 2.6 and 17.1 μg m^{-3} (IQR) with an annual mean of 12.6 (±14.5) μg m^{-3}, much lower than the reported abundance in Kanpur (29−34 μg m^{-3}).[13] The WSOC is a well-accepted tracer of secondary organic aerosols. The WSOC predominately originates through photochemical oxidation of VOCs and primary organic aerosols by different oxidizing species, for example, O_3, OH, and peroxide.[54] However, WSOC may be also emitted directly from the biomass burning,[55] therefore, considered as a marker of smoke emissions coming from biomass/fossil fuel burning.[26] A very high atmospheric abundance of $PM_{1.1}$-bound WSOC was noted with all the measured high concentrations (>13 μg m^{-3}) particularly between late-October and mid-February, overlapping with intense biomass/waste-burning periods over the IGP.[13,45,56] A significant correlation between WSOC and other biomass-burning markers, for example, levoglucosan (r: 0.80); K^+ (r: 0.83); NH_4^+ (r: 0.80); and oxalic acid (r: 0.73), was also noted, reaffirming their common sources over the geographical region.

3.3. $PM_{1.1}$-Bound Elements and CF. Concentrations of measured elements in $PM_{1.1}$ mass and their seasonal variations are shown in Figure 4a, while seasonal differences in $PM_{1.1}$ composition are included in Figure S1 (Supporting Information file). Submicron particulates were metal-enriched having 17% (±6%) of particulate mass being composed of element species with IQR varying from 12 to 20%. Conversely, seasonal variations in elemental enrichment were negligible ranging from 16 ± 5% (pre-monsoon) to 18 ± 7% (winter). Values were comparable to the reported metallic enrichment in Kanpur (5−18%)[57,58] but high against other global cities such as in Barcelona[59] and Mount Cimone, Italy.[60] Clearly, the species such as Ca, Na, Mg, and Fe with signature of crustal and road dust resuspensions contributed the major fractions of particulate mass (12.2%), slightly high during pre-monsoon months (13.1%). Overall, major crustal species (Ca, Na, Mg, and Fe) contributed 72% of total quantified metallic

https://doi.org/10.1021/acsearthspacechem.1c00130
ACS Earth Space Chem. 2021, 5, 2052−2065

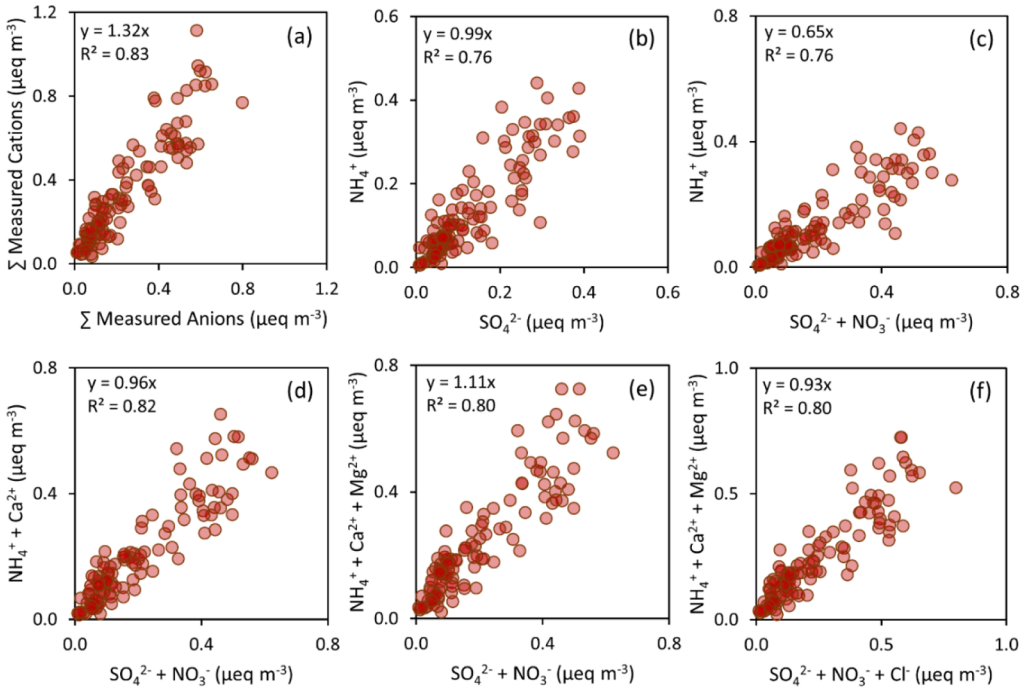

Figure 5. Ionic balance in submicron particulates: (a) measured total cations *vs* total anions, (b) NH_4^+ against SO_4^{2-}, (c) NH_4^+ against SO_4^{2-} and NO_3^-, (d) NH_4^+ and Ca^{2+} against SO_4^{2-} and NO_3^-, (e) NH_4^+, Ca^{2+}, and Mg^{2+} against SO_4^{2-} and NO_3^-, and (f) NH_4^+, Ca^{2+}, and Mg^{2+} against SO_4^{2-}, NO_3^-, and Cl^-.

concentration, while K and Zn contributed the remaining fractions (27%).

Among the species, Ca (4.9 ± 2.3%) and Na (4.6 ± 2.6%) were the most abundant, followed by K (3.4 ± 2.1%), while both Mg (1.7 ± 0.8%) and Zn (1.1 ± 1.4%) were also identified in $PM_{1.1}$. The presence of Ca, Na, Mg, and Fe may be well-traced with crustal/road-dust origin, while the presence of Fe and K in the submicron range is frequently associated to anthropogenic emissions. $PM_{1.1}$-bound K is a typical indicator of biomass-burning smoke but have additional sources such as combustion of residual oil, refuse, and garbage.[45,50] Indiscriminate burning of biomass and refuse/waste is common over this part of the IGP and used both for residential and commercial heating purposes, especially in post-monsoon and winter.[27] Potassium was typically abundant during winter (4.6% of $PM_{1.1}$ mass; IQR: 2.9−7.1 $\mu g\ m^{-3}$) and post-monsoon (3.9%; IQR: 1.3−4.2 $\mu g\ m^{-3}$) compared to pre-monsoon months (2.3%; IQR: 0.3−0.8 $\mu g\ m^{-3}$). The presence of Fe in $PM_{1.1}$ relates contribution from vehicular sources, including engine oil, catalyst-equipped petrol car,[61] and from nonexhaust emissions such as tire and brake wear.[62,63] The presence of Zn was also traced in ambient $PM_{1.1}$ having possible nonexhaust emission sources such as tire wear, industries including smelters, metallurgy, and incinerators, and from burning of waste refuse/garbage.[62,64,65] Among the trace metals, Cr (median: 36 ng m^{-3}), Pb (33 ng m^{-3}), and Cu (5 ng m^{-3}) contributed <1% of particulate mass without any seasonal prevalence (overall IQR: 7−43 ng m^{-3}). Traces of other potential carcinogens (Co, Ni, and Cd) were also evident in $PM_{1.1}$, however, with much less intensity (IQR: 1−4 ng m^{-3}) compared to the neighboring industrial city Kanpur.

The CF and PLI of individual heavy metals were also computed and are included in Figure 4b. The CF, a ratio of measured concentration of a metal to its natural abundance in ambient air (considering US EPA-based ambient metal concentration),[66] indicates the level of enrichment compared to clean air. Overall, for most of the heavy metals, CFs were <1 (low contamination) except for Zn (8.7), Co (3.1), and Cr (2.0). A very high level of Zn enrichment particularly during mid-October to late-February (mean CF: 23.0) indicates its possible emissions from burning of waste refuse/garbage. In contrast, increase in CF for Co and Cr was sporadic, more frequently during pre-monsoon and post-monsoon when westerlies blowing from the upper IGP possibly contribute to local enrichment. The PLI, an indicator of heavy metal contamination of the ambient air, was also computed considering CF of each heavy metal. Except Zn (PLI: 2.04), Co (1.62), and Cr (1.50), PLIs of all the heavy metals were <1, signifying no pollution from these metals to ambient air.

3.4. Water-Soluble Inorganic Species. A significant amount of WSIS was also traced in submicron particulates with an annual mean of 19.7 (±14.8) $\mu g\ m^{-3}$ (IQR: 7.6−33.8 $\mu g\ m^{-3}$; Figure 4c). The WSIS overall contributed 29.5% (±9.1%) of $PM_{1.1}$ mass (IQR: 22.2−35.7%) without much seasonality in terms of their contribution (28−31%). Clearly, particulates were enriched in secondary inorganics such as sulfate, nitrate, and ammonium ions. These secondary ions together contributed a loading of 13.5 (±10.5) $\mu g\ m^{-3}$, contributing 68% (±10%) of total ionic concentration and 20% (±7%) of total particulate mass, slightly high during winter (22%) compared to pre- and post-monsoon seasons (19%). In comparison, secondary inorganics are reported to contribute approximately 30 to 35% of PM_1 mass in Delhi[41] and 40% in Kanpur.[67] These secondary inorganics possibly evolved both through gas- and aqueous-phase photochemical conversion of many aerosol precursors (especially NO_x, SO_2, and NH_3) and eventually neutralized by both ammonium and crustal species.

Among the WSIS, sulfate was the most abundant species (IQR: 2.8−10.9 $\mu g\ m^{-3}$) contributing 10.4% (±4.1%) of particulate mass, followed by nitrate (IQR: 1.1−7.4 $\mu g\ m^{-3}$)

https://doi.org/10.1021/acsearthspacechem.1c00130
ACS Earth Space Chem. 2021, 5, 2052−2065

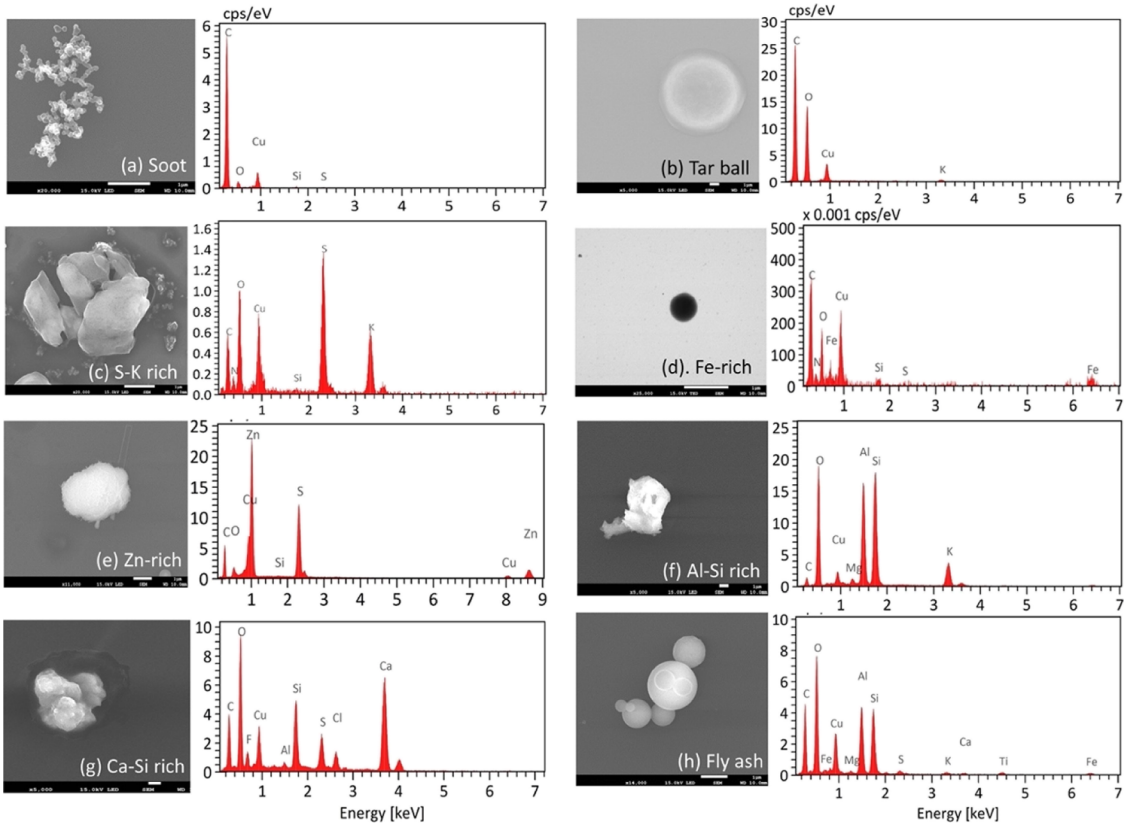

Figure 6. SEM images of various types of particles and their corresponding EDX spectra. Note: A small signal of Cu is due to the use of TEM grids.

accounting 6.0% (±3.1%) of $PM_{1.1}$. Ammonium ions contributed 3.7% (±1.5%) of particulate mass with IQR varying from 1.0 to 3.8 $\mu g\ m^{-3}$. Intraseasonal variations of these secondary ions were significant as they were characteristically high during winter and post-monsoon seasons, owing to their added emissions from biomass/waste-burning emissions compared to summer months. The $PM_{1.1}$-bound NO_3^-/SO_4^{2-} mass ratio, an indicator of relative dominance of mobile sources against stationary sources,[43,68] varied in between 0.3 and 0.6 (IQR) with a mean value of 0.5 (±0.2). This ideally refers to the dominance of stationary sources including biomass/coal/waste/refuse combustion which are well-reported to be important contributors of regional aerosols.[13,45] Besides these secondary WSIS, other ionic species such as Na^+, K^+, Ca^{2+}, and Cl^- shared a fraction of $PM_{1.1}$ mass (8.6%) without much seasonal variations. Potassium ions, a universal tracer of biomass-burning emissions, were enriched in submicron particulate (2.0 ± 1.1% of $PM_{1.1}$ mass; mean concentration ± SD: 1.4 ± 1.2 $\mu g\ m^{-3}$), both during winter (2.1 ± 0.7; 2.4 ± 1.1 $\mu g\ m^{-3}$) and post-monsoon seasons (2.6 ± 1.4; 1.9 ± 1.2 $\mu g\ m^{-3}$). The presence of $PM_{1.1}$-bound Cl^- was also noted (mean ± SD: 1.4 ± 1.3 $\mu g\ m^{-3}$), contributing 2.1% (±1.4) of particulate mass, slightly high during winter compared to the rest of the monitoring period.

3.5. Ionic Balance and Neutralization of Particulate Acidity. Ionic equivalence (Figure 5a) of total measured anions against total cations denotes a strong correlation (R^2: 0.83) with an overall anion deficiency in submicron particulates (slope: 1.32). However, unassessed CO_3^{2-} and HCO_3^- ions may also be a factor of overall anion deficiency.[27] A strong association between NH_4^+ and SO_4^{2-} (R^2: 0.76) and a high NH_4^+/SO_4^{2-} equivalent ratio (0.99) indicate complete neutralization of SO_4^{2-} by NH_4^+ and the formation of $(NH_4)_2SO_4$ and/or NH_4HSO_4. Here, NH_4^+ was insufficient to neutralize all the acidic species as we note the aerosol neutralization ratio, defined as the equivalent molar ratio of NH_4^+ against major acidic species (NO_3^-, SO_4^{2-}, and Cl^-), remained 0.61 ± 0.30. This was in contrast to the neighboring city Kanpur where complete neutralization of aerosol acidity by ammonium was reported by Chakraborty *et al.*[25,67] Considering nitrate neutralization in combination with sulfate ions reduce the slope significantly (0.65, Figure 5c), thus, indicating that metallic cations (such as Ca^{2+}, Mg^{2+}, Na^+, and K^+) also contributed significantly to the aerosol neutralization process (Figure 5d−f). Therefore, the formation of nitrate salt of ammonium and other metallic species may also be a possibility in submicron aerosols. In all three seasons, the neutralization factor of NH_4^+ (0.6−1.0) was higher than that of Ca^{2+} (0.3−0.4) and Mg^{2+} (0.2−0.4), indicating predominate NH_4^+ neutralization (Table S4). However, major metallic cation of crustal origin contributed considerably during pre-monsoon months.

3.6. Morphology and Single-Particle Chemical Characteristics. The single-particle SEM images and the corresponding EDX spectra of individual particles are shown in Figure 6. EDX spectra of 5970 individual particles showed the detection of more than 17 elements with varying extent. The presence of C and O was detected in all the analyzed particles, followed by S (81%), Si (59%), K (48%), and Al (34%), while the rest of the elements were found in less than 20% of the particles. On the basis of elemental composition and morphology, seven particle types were identified that were further classified into four major classes (Table S5). All the

https://doi.org/10.1021/acsearthspacechem.1c00130
ACS Earth Space Chem. 2021, 5, 2052−2065

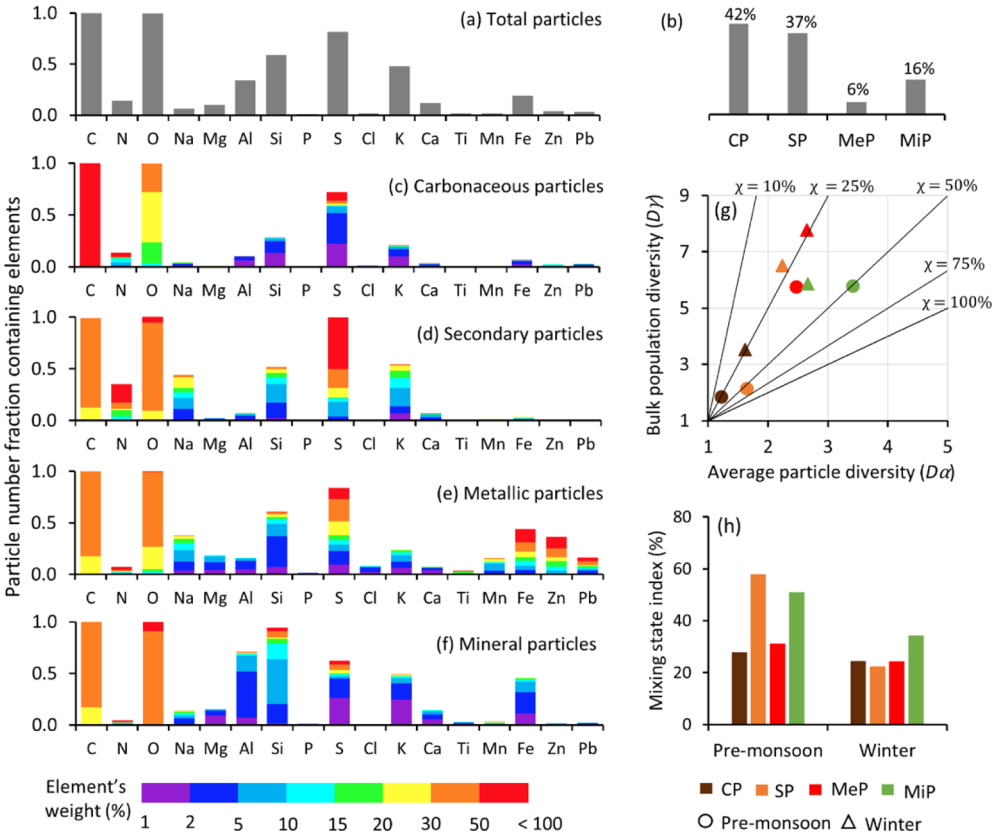

Figure 7. (a) Elemental frequencies in total analyzed particles, (b) contribution of different particle types to total particle number, (c–f) elemental frequencies in different particle classes, (g) average particle and bulk population diversities, and (h) and mixing state indices for different particle classes during pre-monsoon and winter seasons. Note: In (c–f), histogram heights denote the fraction of particles containing a particular element in the particle class and the color represents the weight percent of that element. CPs: carbonaceous particles, SPs: secondary particles, MeP's: metallic particles, MiP's: mineral particles.

major particle types and relative abundance (weight %) of individual element in each particle classes are shown in Figure 7a–f.

Carbonaceous particles (CPs), as in Figure 6a,b, composed primarily of C (element's weight % as in Figure 7c; 50 to <100%) and O (10–50%), with minor quantities of S (1–50%) and K (1–50%), comprised the major fraction (42%) of the submicron particles with insignificant seasonal variations. Soot particles with chain-like agglomerated spherules ranging from small-to-large aggregated clusters were identified (Figure 6a), primarily composed of C with a fraction of O. Significant association of these particles with S was also noted, suggesting their origin from fossil fuel combustion.[69] Another kind of particles having a spherical shape and amorphous with a smooth texture was also spotted that was relatively stable under electron beam (Figure 6b). These particles were devoid of any microstructure and did not form any aggregates, like the typical soot particle does, and were designated as tar balls.[70] Tar balls were present in aged biomass/biofuel-burning emissions[71] and mainly consist of C with minor O and traces of K.[72] The presence of tar balls symbolizes the contribution of biomass and biofuel smoke emissions as combustion of fossil fuels does not typically emit polar organic compounds and polymerize under an ambient environment. Besides soot and tar balls, irregular-shaped particles with C and O along with S, N, and K were also noted and referred to as organic aerosols.

The S- and K-rich particles were grouped as secondary,[73] representing 37% of the total analyzed particles with a high fraction during winter (41%) compared to summer (33%). Secondary particles (SPs) were rich in S (2 to <100%), N (5 to <100%), and K (1–50%) with C (20–50%) and O (20–100%), having an irregular shape and high sensitivity to electron beam (Figure 6c). Association of C- and O-rich particles with S and/or N on the surrounding residue that constituted a liquid coating suggesting more aged aerosols, possibly due to the adsorption and secondary formation of sulfate and/or nitrate.[74]

Metallic particles (MeP's) mainly comprised Fe (Figure 6d) and Zn (Figure 6e), representing 6% of the total particles without much seasonal variations. Fe-rich particles were identified by elemental composition of C (20–50%), O (10 to <100%), and Fe (1 to <100%) with a minor amount of Si, Ti, and Mn, frequently embedded in S- and K-rich particles. The spheroidal shape of Fe-rich particles suggests their anthropogenic origin;[75] thus, they were considered as a tracer for industrial emissions. Zn-bearing particles were of irregular spheroidal shape, composed of Zn-rich coating (5–100%) with other heavy metals.

Particles with the elemental composition of O (30 to <100%), Al (1–50%), and Si (2 to <100%) along with small quantities of Na, Mg, S, K, Ca, Ti, and Fe were grouped as mineral particles (MiP's).[76] The Al–Si-rich particles, however, predominated (Figure 6f–h). MiP's were mostly irregular in shape, with the origin related to the construction activities, resuspension of road dust, and bare soil surfaces.[77] In this group, fly ash composed of O, Al, and Si was also abundant

https://doi.org/10.1021/acsearthspacechem.1c00130
ACS Earth Space Chem. 2021, 5, 2052–2065

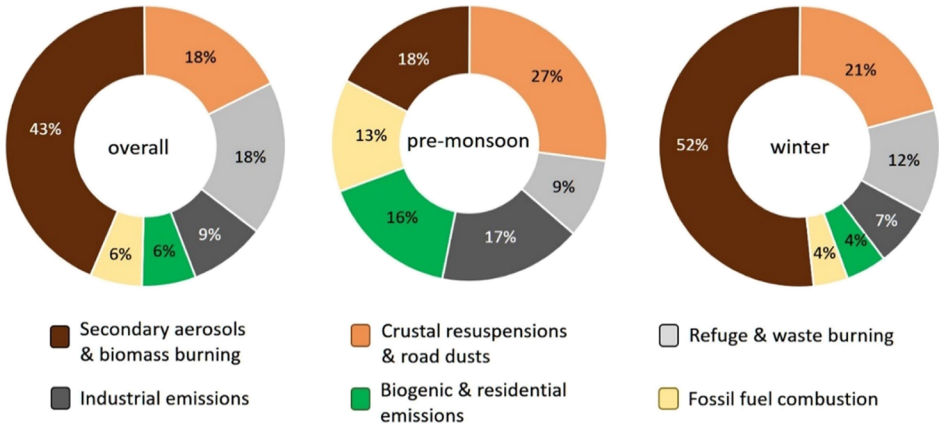

Figure 8. Relative contributions of various emission sources to submicron particulates.

with a spherical shape signifying its possible origin from the high temperature burning. MiP's were frequently coated with S indicating their association with biomass/fuel combustion.[69,78] Overall, MiP's comprised 16% of total particles with greater abundance (18%) during the pre-monsoon period.

3.7. Mixing State of Submicron Particles. In this study, the mixing state of submicron particles was computed based on the mixing entropy concept, defined as the distribution of per-particle chemical species composition.[37,38] Initially, chemical diversity in terms of α and γ diversity was computed before being applied to compute the mixing state index (χ). A mixing state index (χ) close to *zero* indicates an externally mixed aerosols, that is, rather freshly emitted particles. A mixing state index close to *one* refers to internally mixed aerosols, that is, particles with a longer atmospheric time life and have had time to mix with each other resulting in a more uniform particle population.

Here, the lowest average particle diversity (Dα: 1.2−1.6; Figure 7g) was observed for CPs, followed by SPs (Dα: 1.7−2.2), while MiP's (Dα: 2.7−3.4) were highly diverse, followed by MeP's (Dα: 2.5−2.7). An important variability of oxygen and sulfur contents in the carbonaceous aerosols explains a relatively higher bulk diversity Dγ compared to Dα, leading to a mixing state index of 0.24−0.28. This indicates that carbonaceous aerosols, to a certain extent, were externally mixed and freshly emitted. Similarly, MeP's had a mixing state index of 0.24−0.31. This was due to lower average particle chemical diversity than the bulk chemical diversity, so rather externally mixed and freshly emitted particles. CPs had both low particle-specific and bulk diversities, whereas MeP's had considerably both high particle and bulk diversities, this results in a similar range of mixing index. In contrast, SPs were largely internally mixed (χ: 0.58) during pre-monsoon against more externally mixed (χ: 0.22) during winter. The particle-specific diversity for SPs did not vary significantly among the seasons ($D\alpha_{summer}$: 1.7, $D\alpha_{winter}$: 2.2). However, compared to pre-monsoon (Dγ: 2.1), large bulk diversity was observed during winter (Dγ: 6.5) due to fresh emissions from many associated sources[27] which resulted in more externally mixed population (Figure 6h).[37] A similar seasonal discrepancy in mixing state indices of MiP's was also observed ($\chi_{pre\text{-}monsoon}$: 0.51, χ_{winter}: 0.34). Here, bulk diversities were nearly equal ($D\gamma_{summer}$: 5.8, $D\gamma_{winter}$: 5.9) specifying that seasonal variations in the mixing state were mainly due to the average particle diversities ($D\alpha_{summer}$: 3.4, $D\alpha_{winter}$: 2.7).

3.8. Sources of Submicron Particulates. Possible sources of submicron particulates and their relative contribution were assessed (Figure 8) using the PMF model (PMF 5.0), an advanced receptor model based on the weighted least square method.[37,79] A total of 13 elements, 8 WSIS including 3 secondary inorganics (SO_4^{2-}, NO_3^-, and NH_4^+), both anhydrosugars (levoglucosan and galactosan), 19 *n*-alkanes (C_{17}−C_{35}), 5 phthalates, 3 DCAs (C_2, C_3, and C_4), 12 fatty acids (C_{12}−C_{26}), and WSOC were used as input to estimate particulate source contribution. Individual source markers, as noted in Table S6, were selected based on the previous research works over the central IGP[13,27,45,62,67] considering true representativeness of the individual marker to the specific source.

3.8.1. Factor 1: Secondary Aerosols and Biomass-Burning Emissions. Secondary aerosols in combination with biomass-burning emissions were identified as the principal sources of submicron particulates over the central IGP. Secondary aerosols were traced by the presence of secondary inorganics (37−59%; Figure S2) and WSOC (60%) with a fraction of DCA (12−30%). Clearly, biomass-burning emissions also contributed to this factor as marked by the presence of anhydrosugars (44−65%), Cl^- (58%), K^+ (47%), NH_4^+ (37%), and WSOC (60%). An increase in factor 1 contribution during winter (52%) compared to the pre-monsoon (18%) was also noted compared to annual mean (43%).

3.8.2. Factor 2: Crustal Resuspensions and Road Dust. Factor 2 was identified as contributions from crustal resuspensions and road dust based on the presence of Mg^{2+} (56%), Ca^{2+} (51%), Pb (19%), and Zn (24%). Nonexhaust automobile emission sources contribute a significant fraction of airborne Zn,[64,65] while Pb is a typical marker of automobile/road dust.[62,65] Together, these sources contributed 18% of the submicron aerosol mass, slightly high during pre-monsoon (27%) compared to winter months (21%).

3.8.3. Factor 3: Refuse- and Waste-Burning Emissions. Factor 3 with signature of all the major phthalates, Zn (36%), and few HMW *n*-alkanes indicate possible contribution of refuse/waste combustion to $PM_{1.1}$. Burning of solid waste/refuse is frequently practiced in an unscientific and unsegregated manner across the IGP, often in combination with biomass/plant debris in a roadside environment.[29,40] Overall, these sources were found to contribute 18% of $PM_{1.1}$ mass.

3.8.4. Factor 4: Industrial Emissions. The presence of high content of Fe (58%), Cr (46%), Mn (39%), and Co (38%)

https://doi.org/10.1021/acsearthspacechem.1c00130
ACS Earth Space Chem. 2021, 5, 2052−2065

along with few other trace metals (Pb, Cu, and Ni) indicates industrial emissions, mainly from the small-scale metal processing and manufacturing industries. Industrial emissions contributed 9% of airborne $PM_{1.1}$ mass, slightly high during pre-monsoon (17%) compared to the winter period (7%). Seasonal discrepancy in industrial source contribution was possibly induced by the variation in the wind direction as both during summer and winter, westerly prevail over the central IGP, while during summer, an additional contribution of easterly and north-easterly wind may also be noted (Figure S3). Blowing easterly and north-easterly wind during summer carries particulates of industrial origin especially from the mining and quarrying, metal processing, and chemical manufacturing industries, located at Chandauli and Ghazipur districts and possibly contribute to local enrichment of heavy metals.

3.8.5. Factor 5: Biogenic and Residential Emissions. Marked by the presence of fatty acids (42−59%) and HMW *n*-alkanes, the factor 5 indicates the possible contribution of biogenic emissions. However, the presence of few LMW *n*-alkanes with 3 DCAs (C_2, C_3, and C_4: 32−38%) was also noted which relates this also with the emissions from the residential combustion of biomass. Besides, the presence of *n*-HEXDA (49%) and *n*-OCTDA (59%) is associated to cooking emissions.[80] Biogenic and residential combustion emissions were more prominent during summer, possibly due to greater emissions of VOCs from plants,[81] contributing 16% of $PM_{1.1}$ mass against an overall contribution of 6%.

3.8.6. Factor 6: Burning of Fossil Fuels. Factor 6 has a clear signature of emissions from combustion of fossil fuels as significant proportion of this factor is loaded with LMW *n*-alkanes with contribution varying from 54 to 74%. The presence of HMW *n*-alkanes, however, was also noted having characteristic emissions from combustion of fossil fuels including coal. Part of this factor is associated to emissions from brick kilns which are most active during summer. Brick kilns indiscriminately use different fuels including coal, waste plastic, raw biomass, and wood adding much uncertainties to the regional aerosol source profile.[27,29] Burning of fossil fuels overall contributed 6% of $PM_{1.1}$ mass, considerably high during summer months (13%).

The identified sources of submicron particulate and their relative contributions in Varanasi matched well with its neighboring city Kanpur where secondary transformations (46%) with biomass burning (19%) and mineral dust (20%) were reported to be the major PM_1 sources.[13] This even matches well with Delhi with secondary aerosols contributing 50−70% of PM_1 mass.[41] This concludes with a level of certainty that secondary aerosols with precursors from biomass-burning and vehicular/automobile emissions constitute the major fraction of atmospheric submicron particulates over the central IGP which necessitates coordinated actions to safeguard public health.

4. CONCLUSIONS

Submicron particulate database in an urban environment over the central IGP, South Asia, is presented here. The experiment revealed extremely high loadings of submicron particulate with winter and post-monsoon specific peak concentrations. Submicron particulates constituted the major fraction of airborne fine aerosols and the fraction enhanced particularly during extreme pollution days. The constituents of particulate-bound organic aerosols were also assessed. Homologous *n*-alkanes were dominated by the LMW alkanes, with C_{max} at C_{23}. Fatty acids were also traced with prevalence of LMW fatty acids having typical anthropogenic sources. High ratios between C_{sat} [$C_{(18:0+16:0)}$] and C_{unsat} [$C_{(18:n+16:1)}$] suggest the presence of aged aerosols only during summer against relatively fresh aerosols during winter and post-monsoon. Among the anhydrosugars, levoglucosan were dominant during the peak biomass-burning period with a high ratio against its isomer representing emissions from burning of hard wood including agricultural residues. About one-fifth of particulate mass was composed of element species, particularly with Ca, Na, and K. Few trace metals with potential carcinogenicity, for example, Cr, Pb, Co, and Cu, were also identified with a high level of enrichment. Secondary inorganic ions with prevalence of sulfate, nitrate, and ammonium ions constituted 20% of particulate mass. Neutralization of sulfate acidity was primarily associated to ammonium ions favoring the bisulfate formation pathway, while metallic cations also played their part to neutralize total aerosol acidity.

Single-particle analysis indicates that CPs were mostly pure, externally mixed to an extent, and possibly freshly emitted with a coating of sulfur. In contrast, SPs were largely internally mixed during pre-monsoon against externally mixed in winter. Overall, secondary aerosols and biomass-burning emissions were found to be the most important sources of submicron particulates over the central IGP, followed by resuspensions of mineral dusts and burning of refuge/waste. However, a considerable seasonality in the source contributions was also noted.

■ ASSOCIATED CONTENT

Supporting Information

The Supporting Information is available free of charge at https://pubs.acs.org/doi/10.1021/acsearthspacechem.1c00130.

Descriptive statistics of all parameters; mass concentration and diagnostic ratio; abbreviations; neutralization factor; chemical and physical characteristics; markers for source identification; seasonal variation in relative contribution; factor profile; and wind vector (PDF)

■ AUTHOR INFORMATION

Corresponding Author

Tirthankar Banerjee − *Institute of Environment and Sustainable Development and DST-Mahamana Centre of Excellence in Climate Change Research, Banaras Hindu University, Varanasi 742225, India; Laboratoire de Physico-Chimie de l'Atmosphère, Université du Littoral Côte d'Opale, Dunkerque 59140, France;* orcid.org/0000-0002-9717-8248; Email: tb.iesd@bhu.ac.in, tirthankaronline@gmail.com

Authors

Nandita Singh − *Institute of Environment and Sustainable Development, Banaras Hindu University, Varanasi 742225, India; Laboratoire de Physico-Chimie de l'Atmosphère, Université du Littoral Côte d'Opale, Dunkerque 59140, France*

Karine Deboudt − *Laboratoire de Physico-Chimie de l'Atmosphère, Université du Littoral Côte d'Opale, Dunkerque 59140, France*

Abhishek Chakraborty − *Department of Environmental Science & Engineering, Indian Institute of Technology-Bombay, Mumbai 400076, India*
Md Firoz Khan − *Department of Chemistry, Faculty of Science, University of Malaya, Kuala Lumpur 50603, Malaysia;* orcid.org/0000-0003-3567-9634
Mohd Talib Latif − *Department of Earth Sciences and Environment, Universiti Kebangsaan Malaysia, Bangi 43600, Malaysia;* orcid.org/0000-0003-2339-3321

Complete contact information is available at: https://pubs.acs.org/10.1021/acsearthspacechem.1c00130

Author Contributions

N.S.: conceptualization, investigation, formal analysis, writing—original draft, and writing—review and editing. T.B.: conceptualization, investigation, supervision, resource acquisition, writing—original draft, and writing—review and editing. K.D.: analysis and interpretation and writing—review and editing. A.C.: writing—review and editing. M.F.K.: writing—review and editing. M.T.L.: writing—review and editing.

Notes

The authors declare no competing financial interest.

■ ACKNOWLEDGMENTS

This research is partly supported by ASEAN-India S&T Development Fund, Govt. of India (CRD/2018/000011), under ASEAN-India Collaborative Research and Development Scheme. N.S. acknowledges the Department of Science and Technology Women Scientist scheme for doctoral research (SR/WOS-A/EA-1012/2015). Both N.S. and T.B. acknowledge financial support and SEM−EDX research facility offered by LPCA, Université du Littoral Côte d'Opale, to conduct single-particle analysis. LPCA participates in the CaPPA project funded by the ANR through the PIA (contract ANR-11-LABX-0005-01), the "Hauts de France" Regional Council, and the European Regional Development Fund (ERDF). T.B. also acknowledges financial support under IoE Faculty Incentive Grant (6031) from Banaras Hindu University.

■ REFERENCES

(1) Cohen, A. J.; Brauer, M.; Burnett, R.; Anderson, H. R.; Frostad, J.; Estep, K.; Balakrishnan, K.; Brunekreef, B.; Dandona, L.; Dandona, R.; Feigin, V. Estimates and 25-year trends of the global burden of disease attributable to ambient air pollution: an analysis of data from the Global Burden of Diseases Study 2015. *Lancet* **2017**, *389*, 1907−1918.
(2) Singh, N.; Mhawish, A.; Banerjee, T.; Ghosh, S.; Singh, R. S.; Mall, R. K. Association of aerosols, trace gases and black carbon with mortality in an urban pollution hotspot over central Indo-Gangetic Plain. *Atmos. Environ.* **2021**, *246*, 118088.
(3) Lelieveld, J.; Evans, J. S.; Fnais, M.; Giannadaki, D.; Pozzer, A. The contribution of outdoor air pollution sources to premature mortality on a global scale. *Nature* **2015**, *525*, 367−371.
(4) Kanakidou, M.; Myriokefalitakis, S.; Tsigaridis, K. Aerosols in atmospheric chemistry and biogeochemical cycles of nutrients. *Environ. Res. Lett.* **2018**, *13*, 063004.
(5) Myhre, G.; Samset, B. H.; Schulz, M.; Balkanski, Y.; Bauer, S.; Berntsen, T. K.; Bian, H.; Bellouin, N.; Chin, M.; Diehl, T.; Easter, R. C.; Feichter, J.; Ghan, S. J.; Hauglustaine, D.; Iversen, T.; Kinne, S.; Kirkevåg, A.; Lamarque, J.-F.; Lin, G.; Liu, X.; Lund, M. T.; Luo, G.; Ma, X.; van Noije, T.; Penner, J. E.; Rasch, P. J.; Ruiz, A.; Seland, Ø.; Skeie, R. B.; Stier, P.; Takemura, T.; Tsigaridis, K.; Wang, P.; Wang, Z.; Xu, L.; Yu, H.; Yu, F.; Yoon, J.-H.; Zhang, K.; Zhang, H.; Zhou, C. Radiative forcing of the direct aerosol effect from AeroCom Phase II simulations. *Atmos. Chem. Phys.* **2013**, *13*, 1853−1877.
(6) Wang, Y.; Chen, Y. Significant climate impact of highly hygroscopic atmospheric aerosols in Delhi, India. *Geophys. Res. Lett.* **2019**, *46*, 5535−5545.
(7) Seinfeld, J. H.; Bretherton, C.; Carslaw, K. S.; Coe, H.; DeMott, P. J.; Dunlea, E. J.; Feingold, G.; Ghan, S.; Guenther, A. B.; Kahn, R.; Kraucunas, I.; Kreidenweis, S. M.; Molina, M. J.; Nenes, A.; Penner, J. E.; Prather, K. A.; Ramanathan, V.; Ramaswamy, V.; Rasch, P. J.; Ravishankara, A. R.; Rosenfeld, D.; Stephens, G.; Wood, R. Improving our fundamental understanding of the role of aerosol−cloud interactions in the climate system. *Proc. Natl. Acad. Sci. U.S.A.* **2016**, *113*, 5781−5790.
(8) Ramanathan, V.; Chung, C.; Kim, D.; Bettge, T.; Buja, L.; Kiehl, J. T.; Washington, W. M.; Fu, Q.; Sikka, D. R.; Wild, M. Atmospheric brown clouds: Impacts on South Asian climate and hydrological cycle. *Proc. Natl. Acad. Sci. U.S.A.* **2005**, *102*, 5326−5333.
(9) Lau, W. K.; Kim, K. M.; Shi, J. J.; Matsui, T.; Chin, M.; Tan, Q.; Peters-Lidard, C.; Tao, W. K. Impacts of aerosol−monsoon interaction on rainfall and circulation over Northern India and the Himalaya Foothills. *Clim. Dyn.* **2017**, *49*, 1945−1960.
(10) Burney, J.; Ramanathan, V. Recent climate and air pollution impacts on Indian agriculture. *Proc. Natl. Acad. Sci. U.S.A.* **2014**, *111*, 16319−16324.
(11) Sonkar, G.; Mall, R. K.; Banerjee, T.; Singh, N.; Kumar, T. V. L.; Chand, R. Vulnerability of Indian wheat against rising temperature and aerosols. *Environ. Pollut.* **2019**, *254*, 112946.
(12) Hallquist, M.; Wenger, J. C.; Baltensperger, U.; Rudich, Y.; Simpson, D.; Claeys, M.; Dommen, J.; Donahue, N. M.; George, C.; Goldstein, A. H.; Hamilton, J. F.; Herrmann, H.; Hoffmann, T.; Iinuma, Y.; Jang, M.; Jenkin, M. E.; Jimenez, J. L.; Kiendler-Scharr, A.; Maenhaut, W.; McFiggans, G.; Mentel, T. F.; Monod, A.; Prévôt, A. S. H.; Seinfeld, J. H.; Surratt, J. D.; Szmigielski, R.; Wildt, J. The formation, properties and impact of secondary organic aerosol: current and emerging issues. *Atmos. Chem. Phys.* **2009**, *9*, 5155−5236.
(13) Rajput, P.; Singh, D. K.; Singh, A. K.; Gupta, T. Chemical composition and source-apportionment of sub-micron particles during wintertime over Northern India: New insights on influence of fog-processing. *Environ. Pollut.* **2018**, *233*, 81−91.
(14) Zhang, Q.; Jimenez, J. L.; Canagaratna, M. R.; Ulbrich, I. M.; Ng, N. L.; Worsnop, D. R.; Sun, Y. Understanding atmospheric organic aerosols via factor analysis of aerosol mass spectrometry: a review. *Anal. Bioanal. Chem.* **2011**, *401*, 3045−3067.
(15) Chakraborty, A.; Gupta, T. Chemical characterization and source apportionment of submicron (PM1) aerosol in Kanpur region, India. *Aerosol Air Qual. Res.* **2010**, *10*, 433−445.
(16) Bari, M. A.; Kindzierski, W. B.; Wallace, L. A.; Wheeler, A. J.; MacNeill, M.; Héroux, M.-È. Indoor and outdoor levels and sources of submicron particles (PM1) at homes in Edmonton, Canada. *Environ. Sci. Technol.* **2015**, *49*, 6419−6429.
(17) Esposito, V.; Lucariello, A.; Savarese, L.; Cinelli, M. P.; Ferraraccio, F.; Bianco, A.; De Luca, A.; Mazzarella, G. Morphology changes in human lung epithelial cells after exposure to diesel exhaust micron sub particles (PM1. 0) and pollen allergens. *Environ. Pollut.* **2012**, *171*, 162−167.
(18) Pérez, N.; Pey, J.; Reche, C.; Cortés, J.; Alastuey, A.; Querol, X. Impact of harbour emissions on ambient PM10 and PM2. 5 in Barcelona (Spain): Evidences of secondary aerosol formation within the urban area. *Sci. Total Environ.* **2016**, *571*, 237−250.
(19) Breitner, S.; Liu, L.; Cyrys, J.; Brüske, I.; Franck, U.; Schlink, U.; Leitte, A. M.; Herbarth, O.; Wiedensohler, A.; Wehner, B.; Hu, M.; Pan, X.-C.; Wichmann, H.-E.; Peters, A. Sub-micrometer particulate air pollution and cardiovascular mortality in Beijing, China. *Sci. Total Environ.* **2011**, *409*, 5196−5204.
(20) Banerjee, T.; Shitole, A. S.; Mhawish, A.; Anand, A.; Ranjan, R.; Khan, M. F.; Srithawirat, T.; Latif, M. T.; Mall, R. K. Aerosol climatology over South and Southeast Asia: Aerosol types, vertical profile and source fields. *J. Geophys. Res.: Atmos.* **2021**, *126*, No. e2020JD033554.

(21) Sen, A.; Abdelmaksoud, A. S.; Nazeer Ahammed, Y.; Alghamdi, M. A.; Banerjee, T.; Bhat, M. A.; et al. Variations in particulate matter over Indo-Gangetic Plains and Indo-Himalayan Range during four field campaigns in winter monsoon and summer monsoon: role of pollution pathways. *Atmos. Environ.* **2017**, *154*, 200−224.
(22) Gautam, R.; Hsu, N. C.; Tsay, S. C.; Lau, K. M.; Holben, B.; Bell, S.; Smirnov, A.; Li, C.; Hansell, R.; Ji, Q.; Payra, S.; Aryal, D.; Kayastha, R.; Kim, K. M. Accumulation of aerosols over the Indo-Gangetic plains and southern slopes of the Himalayas: distribution, properties and radiative effects during the 2009 pre-monsoon season. *Atmos. Chem. Phys.* **2011**, *11*, 12841−12863.
(23) Mhawish, A.; Banerjee, T.; Broday, D. M.; Misra, A.; Tripathi, S. N. Evaluation of MODIS Collection 6 aerosol retrieval algorithms over Indo-Gangetic Plain: Implications of aerosols types and mass loading. *Remote Sens. Environ.* **2017**, *201*, 297−313.
(24) Mhawish, A.; Vinjamuri, K. S.; Singh, N.; Kumar, M.; Banerjee, T. Vertical Profiling of Aerosol and Aerosol Types Using Space-Borne Lidar. *Measurement, Analysis and Remediation of Environmental Pollutants*; Springer: Singapore, 2020; pp 165−177.
(25) Chakraborty, A.; Bhattu, D.; Gupta, T.; Tripathi, S. N.; Canagaratna, M. R. Real-time measurements of ambient aerosols in a polluted Indian city: Sources, characteristics, and processing of organic aerosols during foggy and nonfoggy periods. *J. Geophys. Res.: Atmos.* **2015**, *120*, 9006−9019.
(26) Singh, N.; Mhawish, A.; Deboudt, K.; Singh, R. S.; Banerjee, T. Organic aerosols over Indo-Gangetic Plain: Sources, distributions and climatic implications. *Atmos. Environ.* **2017**, *157*, 59−74.
(27) Singh, N.; Banerjee, T.; Murari, V.; Deboudt, K.; Khan, M. F.; Singh, R. S.; Latif, M. T. Insights into size-segregated particulate chemistry and sources in urban environment over central Indo-Gangetic Plain. *Chemosphere* **2021**, *263*, 128030.
(28) Jain, S.; Sharma, S. K.; Vijayan, N.; Mandal, T. K. Seasonal characteristics of aerosols (PM2. 5 and PM10) and their source apportionment using PMF: a four year study over Delhi, India. *Environ. Pollut.* **2020**, *262*, 114337.
(29) Murari, V.; Singh, N.; Ranjan, R.; Singh, R. S.; Banerjee, T. Source apportionment and health risk assessment of airborne particulates over central Indo-Gangetic Plain. *Chemosphere* **2020**, *257*, 127145.
(30) Singh, D. K.; Gupta, T. Role of transition metals with water soluble organic carbon in the formation of secondary organic aerosol and metallo-organics in PM1 sampled during post monsoon and pre-winter time. *J. Aerosol Sci.* **2016**, *94*, 56−69.
(31) Kaul, D. S.; Gupta, T.; Tripathi, S. N.; Tare, V.; Collett, J. L., Jr. Secondary organic aerosol: a comparison between foggy and nonfoggy days. *Environ. Sci. Technol.* **2011**, *45*, 7307−7313.
(32) Ramana, M. V.; Ramanathan, V.; Feng, Y.; Yoon, S.-C.; Kim, S.-W.; Carmichael, G. R.; Schauer, J. J. Warming influenced by the ratio of black carbon to sulphate and the black-carbon source. *Nat. Geosci.* **2010**, *3*, 542−545.
(33) Hu, Q. H.; Xie, Z. Q.; Wang, X. M.; Kang, H.; Zhang, P. Levoglucosan indicates high levels of biomass burning aerosols over oceans from the Arctic to Antarctic. *Sci. Rep.* **2013**, *3*, 3119.
(34) EPA. *National Air Quality and Emissions Trends Report*; Office of Air Quality Planning and Standards, 1999.
(35) Kirillova, E. N.; Sheesley, R. J.; Andersson, A.; Gustafsson, O. Natural abundance 13C and 14C analysis of water-soluble organic carbon in atmospheric aerosols. *Anal. Chem.* **2010**, *82*, 7973−7978.
(36) Okada, K.; Ikegami, M.; Zaizen, Y.; Tsutsumi, Y.; Makino, Y.; Jensen, J. B.; Gras, J. L. Soot particles in the free troposphere over Australia. *Atmos. Environ.* **2005**, *39*, 5079−5089.
(37) Riemer, N.; West, M. Quantifying aerosol mixing state with entropy and diversity measures. *Atmos. Chem. Phys.* **2013**, *13*, 11423−11439.
(38) Riemer, N.; Ault, A. P.; West, M.; Craig, R. L.; Curtis, J. H. Aerosol mixing state: measurements, modeling, and impacts. *Rev. Geophys.* **2019**, *57*, 187−249.
(39) Khan, M. F.; Latif, M. T.; Saw, W. H.; Amil, N.; Nadzir, M. S. M.; Sahani, M.; Tahir, N. M.; Chung, J. X. Fine particulate matter in the tropical environment: monsoonal effects, source apportionment, and health risk assessment. *Atmos. Chem. Phys.* **2016**, *16*, 597−617.
(40) Banerjee, T.; Kumar, M.; Mall, R. K.; Singh, R. S. Airing 'clean air' in clean India mission. *Environ. Sci. Pollut. Res.* **2017**, *24*, 6399−6413.
(41) Gani, S.; Bhandari, S.; Seraj, S.; Wang, D. S.; Patel, K.; Soni, P.; Arub, Z.; Habib, G.; Hildebrandt Ruiz, L.; Apte, J. S. Submicron aerosol composition in the world's most polluted megacity: the Delhi Aerosol Supersite study. *Atmos. Chem. Phys.* **2019**, *19*, 6843−6859.
(42) Chen, S.; Zhao, Y.; Zhang, R. Formation Mechanism of Atmospheric Ammonium Bisulfate: Hydrogen-Bond-Promoted Nearly Barrierless Reactions of SO3 with NH3 and H2O. *ChemPhysChem* **2018**, *19*, 967−972.
(43) Zhang, J.-S.; Gui, Z.-H.; Zou, Z.-Y.; Yang, B.-Y.; Ma, J.; Jing, J.; Wang, H.-J.; Luo, J.-Y.; Zhang, X.; Luo, C.-Y.; Wang, H.; Zhao, H.-P.; Pan, D.-H.; Bao, W.-W.; Guo, Y.-M.; Ma, Y.-H.; Dong, G.-H.; Chen, Y.-J. Long-term exposure to ambient air pollution and metabolic syndrome in children and adolescents: A national cross-sectional study in China. *Environ. Int.* **2021**, *148*, 106383.
(44) Samek, L.; Stegowski, Z.; Styszko, K.; Furman, L.; Fiedor, J. Seasonal contribution of assessed sources to submicron and fine particulate matter in a Central European urban area. *Environ. Pollut.* **2018**, *241*, 406−411.
(45) Singh, N.; Banerjee, T.; Raju, M. P.; Deboudt, K.; Sorek-Hamer, M.; Singh, R. S.; Mall, R. K. Aerosol chemistry, transport, and climatic implications during extreme biomass burning emissions over the Indo-Gangetic Plain. *Atmos. Chem. Phys.* **2018**, *18*, 14197−14215.
(46) Ren, L.; Fu, P.; He, Y.; Hou, J.; Chen, J.; Pavuluri, C. M.; Sun, Y.; Wang, Z. Molecular distributions and compound-specific stable carbon isotopic compositions of lipids in wintertime aerosols from Beijing. *Sci. Rep.* **2016**, *6*, 27481.
(47) Fu, P.; Kawamura, K.; Miura, K. Molecular characterization of marine organic aerosols collected during a round-the-world cruise. *J. Geophys. Res.: Atmos.* **2011**, *116*, D13302.
(48) Rogge, W. F.; Medeiros, P. M.; Simoneit, B. R. T. Organic marker compounds for surface soil and fugitive dust from open lot dairies and cattle feedlots. *Atmos. Environ.* **2006**, *40*, 27−49.
(49) Gadi, R.; Shivani, S. K.; Sharma, S. K.; Mandal, T. K. Source apportionment and health risk assessment of organic constituents in fine ambient aerosols (PM2. 5): a complete year study over National Capital Region of India. *Chemosphere* **2019**, *221*, 583−596.
(50) Cheng, Y.; Engling, G.; He, K.-B.; Duan, F.-K.; Ma, Y.-L.; Du, Z.-Y.; Liu, J.-M.; Zheng, M.; Weber, R. J. Biomass burning contribution to Beijing aerosol. *Atmos. Chem. Phys.* **2013**, *13*, 7765−7781.
(51) Sorathia, F.; Rajput, P.; Gupta, T. Dicarboxylic acids and levoglucosan in aerosols from Indo-Gangetic Plain: Inferences from day night variability during wintertime. *Sci. Total Environ.* **2018**, *624*, 451−460.
(52) Li, J.; Wang, G.; Aggarwal, S. G.; Huang, Y.; Ren, Y.; Zhou, B.; Singh, K.; Gupta, P. K.; Cao, J.; Zhang, R. Comparison of abundances, compositions and sources of elements, inorganic ions and organic compounds in atmospheric aerosols from Xi'an and New Delhi, two megacities in China and India. *Sci. Total Environ.* **2014**, *476*, 485−495.
(53) Fu, P.; Kawamura, K.; Okuzawa, K.; Aggarwal, S. G.; Wang, G.; Kanaya, Y.; Wang, Z. Organic molecular compositions and temporal variations of summertime mountain aerosols over Mt. Tai, North China Plain. *J. Geophys. Res.: Atmos.* **2008**, *113*, D19107.
(54) Chang, S.-C.; Lee, C.-T. Secondary aerosol formation through photochemical reactions estimated by using air quality monitoring data in Taipei City from 1994 to 2003. *Atmos. Environ.* **2007**, *41*, 4002−4017.
(55) Weber, R. J.; Sullivan, A. P.; Peltier, R. E.; Russell, A.; Yan, B.; Zheng, M.; De Gouw, J.; Warneke, C.; Brock, C.; Holloway, J. S.; Atlas, E. L. A study of secondary organic aerosol formation in the anthropogenic-influenced southeastern United States. *J. Geophys. Res.: Atmos.* **2007**, *112*, D13302.

https://doi.org/10.1021/acsearthspacechem.1c00130
ACS Earth Space Chem. 2021, 5, 2052−2065

(56) Kumar, M.; Raju, M. P.; Singh, R. K.; Singh, A. K.; Singh, R. S.; Banerjee, T. Wintertime characteristics of aerosols over middle Indo-Gangetic Plain: Vertical profile, transport and radiative forcing. *Atmos. Res.* **2017**, *183*, 268−282.
(57) Izhar, S.; Goel, A.; Chakraborty, A.; Gupta, T. Annual trends in occurrence of submicron particles in ambient air and health risk posed by particle bound metals. *Chemosphere* **2016**, *146*, 582−590.
(58) Rajput, P.; Mandaria, A.; Kachawa, L.; Singh, D. K.; Singh, A. K.; Gupta, T. Chemical characterisation and source apportionment of PM1 during massive loading at an urban location in Indo-Gangetic Plain: impact of local sources and long-range transport. *Tellus B* **2016**, *68*, 30659.
(59) Pérez, N.; Pey, J.; Castillo, S.; Viana, M.; Alastuey, A.; Querol, X. Interpretation of the variability of levels of regional background aerosols in the Western Mediterranean. *Sci. Total Environ.* **2008**, *407*, 527−540.
(60) Marenco, F.; Bonasoni, P.; Calzolari, F.; Ceriani, M.; Chiari, M.; Cristofanelli, P.; D'Alessandro, A.; Fermo, P.; Lucarelli, F.; Mazzei, F.; Nava, S. Characterization of atmospheric aerosols at Monte Cimone, Italy, during summer 2004: source apportionment and transport mechanisms. *J. Geophys. Res.: Atmos.* **2006**, *111*, D24202.
(61) Chen, C.; Huang, C.; Jing, Q.; Wang, H.; Pan, H.; Li, L.; Zhao, J.; Dai, Y.; Huang, H.; Schipper, L.; Streets, D. G. On-road emission characteristics of heavy-duty diesel vehicles in Shanghai. *Atmos. Environ.* **2007**, *41*, 5334−5344.
(62) Banerjee, T.; Murari, V.; Kumar, M.; Raju, M. P. Source apportionment of airborne particulates through receptor modeling: Indian scenario. *Atmos. Res.* **2015**, *164*, 167−187.
(63) Kukutschová, J.; Moravec, P.; Tomášek, V.; Matějka, V.; Smolík, J.; Schwarz, J.; Seidlerová, J.; Šafářová, K.; Filip, P. On airborne nano/micro-sized wear particles released from low-metallic automotive brakes. *Environ. Pollut.* **2011**, *159*, 998−1006.
(64) Font, A.; de Hoogh, K.; Leal-Sanchez, M.; Ashworth, D. C.; Brown, R. J. C.; Hansell, A. L.; Fuller, G. W. Using metal ratios to detect emissions from municipal waste incinerators in ambient air pollution data. *Atmos. Environ.* **2015**, *113*, 177−186.
(65) Lough, G. C.; Schauer, J. J.; Park, J.-S.; Shafer, M. M.; DeMinter, J. T.; Weinstein, J. P. Emissions of metals associated with motor vehicle roadways. *Environ. Sci. Technol.* **2005**, *39*, 826−836.
(66) Geiger, A.; Cooper, J. *Overview of Airborne Metals Regulations, Exposure Limits, Health Effects, and Contemporary Research*; US Environmental Protection Agency, 2010.
(67) Chakraborty, A.; Rajeev, P.; Rajput, P.; Gupta, T. Water soluble organic aerosols in indo gangetic plain (IGP): Insights from aerosol mass spectrometry. *Sci. Total Environ.* **2017**, *599*, 1573−1582.
(68) Tian, M.; Wang, H.; Chen, Y.; Yang, F.; Zhang, X.; Zou, Q.; Zhang, R.; Ma, Y.; He, K. Characteristics of aerosol pollution during heavy haze events in Suzhou, China. *Atmos. Chem. Phys.* **2016**, *16*, 7357−7371.
(69) Campos-Ramos, A.; Aragón-Piña, A.; Galindo-Estrada, I.; Querol, X.; Alastuey, A. Characterization of atmospheric aerosols by SEM in a rural area in the western part of México and its relation with different pollution sources. *Atmos. Environ.* **2009**, *43*, 6159−6167.
(70) Pósfai, M.; Gelencsér, A.; Simonics, R.; Arató, K.; Li, J.; Hobbs, P. V.; Buseck, P. R. Atmospheric tar balls: Particles from biomass and biofuel burning. *J. Geophys. Res.: Atmos.* **2004**, *109*, D06213.
(71) Alfaro, S. C.; Gaudichet, A.; Rajot, J. L.; Gomes, L.; Maillé, M.; Cachier, H. Variability of aerosol size-resolved composition at an Indian coastal site during the Indian Ocean Experiment (INDOEX) intensive field phase. *J. Geophys. Res.: Atmos.* **2003**, *108*, 4235.
(72) Chen, Y.; Shah, N.; Braun, A.; Huggins, F. E.; Huffman, G. P. Electron microscopy investigation of carbonaceous particulate matter generated by combustion of fossil fuels. *Energy Fuels* **2005**, *19*, 1644−1651.
(73) Vester, B.; Ebert, M.; Barnert, E.; Schneider, J.; Kandler, K.; Schütz, L.; Weinbruch, S. Composition and mixing state of the urban background aerosol in the Rhein-Main area (Germany). *Atmos. Environ.* **2007**, *41*, 6102−6115.
(74) Craig, R. L.; Bondy, A. L.; Ault, A. P. Computer-controlled Raman microspectroscopy (CC-Raman): A method for the rapid characterization of individual atmospheric aerosol particles. *Aerosol Sci. Technol.* **2017**, *51*, 1099−1112.
(75) Xie, R. K.; Seip, H. M.; Leinum, J. R.; Winje, T.; Xiao, J. S. Chemical characterization of individual particles (PM10) from ambient air in Guiyang City, China. *Sci. Total Environ.* **2005**, *343*, 261−272.
(76) Deboudt, K.; Flament, P.; Choël, M.; Gloter, A.; Sobanska, S.; Colliex, C. Mixing state of aerosols and direct observation of carbonaceous and marine coatings on African dust by individual particle analysis. *J. Geophys. Res.: Atmos.* **2010**, *115*, D24207.
(77) Murari, V.; Kumar, M.; Barman, S. C.; Banerjee, T. Temporal variability of MODIS aerosol optical depth and chemical characterization of airborne particulates in Varanasi, India. *Environ. Sci. Pollut. Res.* **2015**, *22*, 1329−1343.
(78) Paoletti, L.; De Berardis, B.; Arrizza, L.; Passacantando, M.; Inglessis, M.; Mosca, M. Seasonal effects on the physico-chemical characteristics of PM2. 1 in Rome: a study by SEM and XPS. *Atmos. Environ.* **2003**, *37*, 4869−4879.
(79) Cesari, D.; De Benedetto, G. E.; Bonasoni, P.; Busetto, M.; Dinoi, A.; Merico, E.; Chirizzi, D.; Cristofanelli, P.; Donateo, A.; Grasso, F. M.; Marinoni, A.; Pennetta, A.; Contini, D. Seasonal variability of PM2. 5 and PM10 composition and sources in an urban background site in Southern Italy. *Sci. Total Environ.* **2018**, *612*, 202−213.
(80) Fine, P. M.; Chakrabarti, B.; Krudysz, M.; Schauer, J. J.; Sioutas, C. Diurnal variations of individual organic compound constituents of ultrafine and accumulation mode particulate matter in the Los Angeles basin. *Environ. Sci. Technol.* **2004**, *38*, 1296−1304.
(81) Padhy, P. K.; Varshney, C. K. Emission of volatile organic compounds (VOC) from tropical plant species in India. *Chemosphere* **2005**, *59*, 1643−1653.

https://doi.org/10.1021/acsearthspacechem.1c00130
ACS Earth Space Chem. 2021, 5, 2052−2065